

# Biomembrane Force Probe (BFP): Designs, advancements and recent applications to live-cell mechanobiology

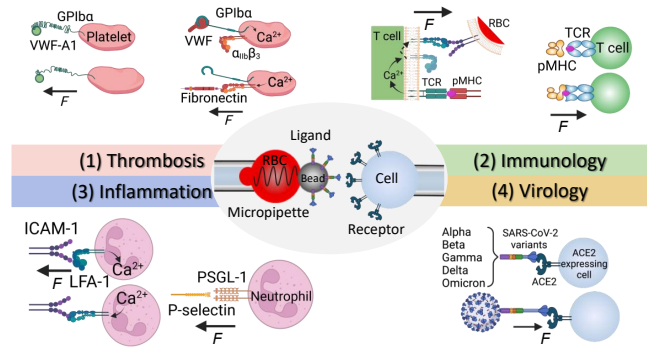
Laura Moldovan<sup>1</sup>, Caroline Song<sup>1</sup>, Catherine Chen<sup>1</sup>, Jerry Wang<sup>1</sup>, and Lining Arnold Ju<sup>1</sup>

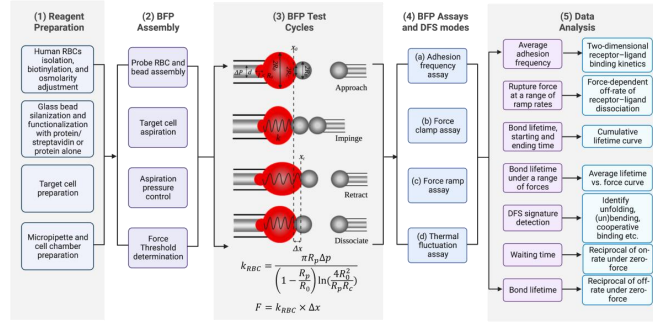
<sup>1</sup>The University of Sydney

February 23, 2023

## Abstract

Mechanical forces play a crucial role in biological processes at the molecular and cellular levels. Recent advancements in dynamic force spectroscopies (DFS) have enabled the application and measurement of forces and displacements with high resolutions, providing insights into the mechanical pathways involved in various diseases, including cancer, cardiovascular disease, and COVID-19. Among the various DFS techniques, biomembrane force probe (BFP) advancements have improved our ability to measure bond kinetics and cellular mechanosensing with pico-newton and nano-meter resolutions. In this review, we provide a comprehensive overview of the classical BFP-DFS setup and highlight key advancements, including the development of dual biomembrane force probe (dBFP) and fluorescence biomembrane force probe (fBFP). BFP-DFS not only enables the investigation of dynamic bond behaviors on living cells, but also contributed significantly to our understanding of the specific ligand–receptor axes mediated cell mechanosensing. Besides, we explore the contribution of discoveries made possible by BFP-DFS in cancer biology, thrombosis, and inflammation, as well as predict future BFP upgrades to improve output and feasibility. Although BFP-DFS is still a niche research modality, its contribution to the growing field of cell mechanobiology is unparalleled, and its potential to elucidate novel therapeutic discoveries is significant.





## **Abstract**

Mechanical forces play a crucial role in biological processes at the molecular and cellular levels. Recent advancements in dynamic force spectroscopies (DFS) have enabled the application and measurement of forces and displacements with high resolutions, providing insights into the mechanical pathways involved in various diseases, including cancer, cardiovascular disease, and COVID-19. Among the various DFS techniques, biomembrane force probe (BFP) advancements have improved our ability to measure bond kinetics and cellular mechanosensing with pico-newton and nano-meter resolutions. In this review, we provide a comprehensive overview of the classical BFP-DFS setup and highlight key advancements, including the development of dual biomembrane force probe (dBFP) and fluorescence biomembrane force probe (fBFP). BFP-DFS not only enables the investigation of dynamic bond behaviors on living cells, but also contributed significantly to our understanding of the specific ligand–receptor axes mediated cell mechanosensing. Besides, we explore the contribution of discoveries made possible by BFP-DFS in cancer biology, thrombosis, and inflammation, as well as predict future BFP upgrades to improve output and feasibility. Although BFP-DFS is still a niche research modality, its contribution to the growing field of cell mechanobiology is unparalleled, and its potential to elucidate novel therapeutic discoveries is significant.

# **Biomembrane Force Probe (BFP): Designs, advancements and recent applications to live-cell mechanobiology**

Laura Moldovan<sup>1,2,3,\*</sup>, Caroline Haoran Song<sup>1,2,3,4,\*</sup>, Catherine Yiyao Chen<sup>1,\*</sup>, Jerry Haoqing Wang<sup>1,3,4</sup>, Lining Arnold Ju<sup>1,2,3,4,†</sup>

<sup>1</sup> School of Biomedical Engineering, The University of Sydney, Darlington, NSW 2008, Australia

<sup>2</sup> Charles Perkins Centre, The University of Sydney, Camperdown, NSW 2006, Australia

<sup>3</sup> Heart Research Institute, Camperdown, Newtown, NSW 2042, Australia.

<sup>4</sup> The University of Sydney Nano Institute (Sydney Nano), The University of Sydney, Camperdown, NSW 2006, Australia

\*These authors contributed equally

†Correspondence: Arnold.ju@sydney.edu.au

## **Abstract**

Mechanical forces play a crucial role in biological processes at the molecular and cellular levels. Recent advancements in dynamic force spectroscopies (DFS) have enabled the application and measurement of forces and displacements with high resolutions, providing insights into the mechanical pathways involved in various diseases, including cancer, cardiovascular disease, and COVID-19. Among the various DFS techniques, biomembrane force probe (BFP) advancements have improved our ability to measure bond kinetics and cellular mechanosensing with pico-newton and nano-meter resolutions. In this review, we provide a comprehensive overview of the classical BFP-DFS setup and highlight key advancements, including the development of dual biomembrane force probe (dBFP) and fluorescence biomembrane force probe (fBFP). BFP-DFS not only enables the investigation of dynamic bond behaviors on living cells, but also contributed significantly to our understanding of the specific ligand–receptor axes mediated cell mechanosensing. Besides, we explore the contribution of discoveries made possible by BFP-DFS in cancer biology, thrombosis, and inflammation, as well as predict future BFP upgrades to improve output and feasibility. Although BFP-DFS is still a niche research modality, its contribution to the growing field of cell mechanobiology is unparalleled, and its potential to elucidate novel therapeutic discoveries is significant.

## **1. Introduction**

Interest in the field of mechanobiology has grown significantly over the past few years. Mechanobiology describes the interplay between single cells and their mechanical environment, and emerges at the intersection of medicine, biology, biophysics, and engineering<sup>1</sup>. New discoveries in the field of mechanobiology have been made possible, in large part, due to advances in dynamic force spectroscopy (DFS) performed with micromanipulation techniques, including atomic force microscopy (AFM), optical trap (OT), and biomembrane force probe (BFP)<sup>2</sup>. Recent developments in the BFP technology have enabled biomechanical analysis at both the microscale (single cell) and nanoscale (single molecule) levels, providing insight into mechanisms underlying a wide range of biological processes related to prevalent human diseases including cancer, thrombosis, and inflammation (Figure 1). Recently, BFP was even used to elucidate the mechanical activation of spike protein on SARS-CoV-2 viral infection<sup>3</sup>. Further, over the past two decades, DFS coupled with BFP has provided various biomechanical approaches for manipulation, characterization, and

visualization of single ligand-receptor interactions and conformational changes with subsequent signalling events on live cells<sup>4,5</sup>.

Stemming from micropipette aspiration techniques, the BFP was initially developed by Evan Evans in the mid-1990s with the intent to investigate the strength of single molecular bonds under sub-microscopic forces at biological interfaces<sup>6</sup>. Over the past decade, BFP systems have been established by several groups, and the technical details have been reviewed alongside other nanotools<sup>2,7-9</sup>. The conventional BFP setup is represented in Figure 1 and consists of two opposing micropipettes aligned along their horizontal axis' (*left*: 'Probe'; *right*: 'Target'). While the in-house setups may vary slightly, the basic structure of each BFP is similar. The left micropipette, which is held stationary, aspirates a biotinylated human red blood cell (RBC) with a streptavidin-coated glass microbead on its apex, which can be coated with ligands of interest (Figure 1). On the right, another micropipette, controlled by a piezoelectric translator holds the opposing bead or cell bearing complementary receptors and is driven to impinge the probe bead in a repeated approach-push-retract-hold-return test cycle<sup>10</sup>. A third micropipette (termed 'Helper') is typically utilized to attach the streptavidin-coated glass bead onto the apex of the RBC. When pressurized by micropipette aspiration, the RBC serves as an ultrasensitive force transducer. Typically, the BFP is configured with at least two cameras, an inverted microscope with a dry objective lens (e.g., 40X/NA0.75), a mercury lamp as a light source, and several video tubes. One camera operates at high speed to track the displacement of the RBC-Probe edge, while the other allows real-time visualization of the ongoing experiment<sup>11</sup>. Enabled by fast video processing, the RBC-Probe edge is tracked along the pulling direction at a video rate of up to 1600 fps when the images are limited to a 24-30-line strip across the bead<sup>12</sup>.

Over the past 20 years, BFP has been utilized as a dynamic force spectroscopy (DFS) technique to continuously contribute to the field of mechanobiology by providing high resolution in position, time, and force (2-5 nm, 0.3-0.5 ms, and 0.2-0.5 pN)<sup>13</sup>. Aside from the conventional BFP, advancements in the setup have led to the development of both a dual BFP and fluorescent BFP setup. The BFP-DFS applications include but are not limited to ligand binding kinetics<sup>14-19</sup>, cytoskeleton mediated receptor activation<sup>20-24</sup>, 2D receptor conformational changes<sup>25,26</sup> and dual receptor crosstalk<sup>27,28</sup>. More broadly, the elucidation of these mechanisms has contributed significantly to research in the fields of cancer biology, thrombosis, and inflammation.

Ultimately, the BFP is a sensitive technique that has grown significantly in scope and application over the past few decades. In this review, we first introduce the conventional BFP and further elaborate on updated techniques using this technology. We then highlight the versatility of BFP, summarizing a few key upgrades and their impact on the field of mechanobiology. Further, we explore the novel clinical contributions made possible by this technique in the context of cancer biology, thrombosis, and inflammation. Finally, we propose potential developments and future implications in the field

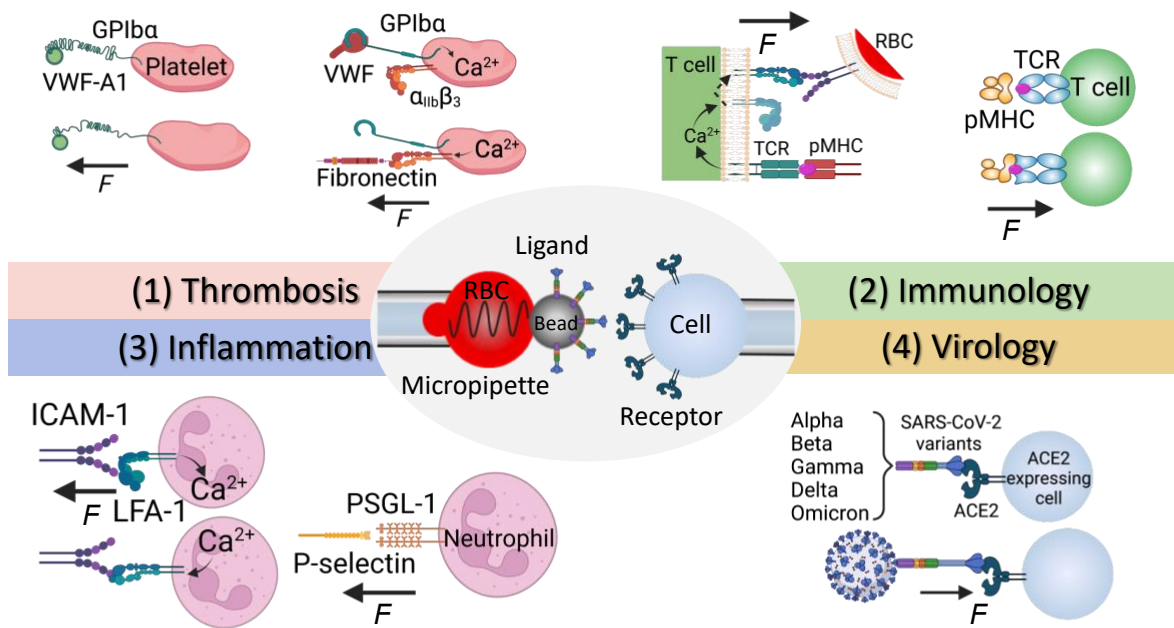


**Figure 1 Biomembrane Force Probe (BFP): Design, advancements, and mechanobiological application.** Schematic of the biomembrane force probe (BFP) (*center*). The probe micropipette (*left*) aspirates a biotinylated human red blood cell (RBC) with a ligand-bearing glass microbead attached to its apex. The RBC serves as a force transducer whose spring constant can be adjusted. The target micropipette (*right*) aspirates a complimentary receptor-bearing cell and is brought to impinge the probe microbead, during which one or more bonds may form. The BFP technique has broad applications in several fields, including: **(1) Thrombosis**, which involves the unfolding of platelet receptor glycoprotein Iba (GPIIb) upon interaction with von Willebrand factor (VWF) A1 domain under force<sup>17,26,29,30</sup> (*left*) and the conformational change of platelet integrin  $\alpha_{IIb}\beta_3$  from bent-closed to extended-closed upon interaction with fibronectin after VWF interaction<sup>28,31,32</sup> (*right*); **(2) Immunology**, which involves the subunit rotation of T-cell receptor (TCR) when impinged by ligand peptide-bound MHC (pMHC)<sup>19,33</sup> (*left*), and the conformational change of

lymphocyte function-associated antigen 1 (LFA-1) from closed to extended when impinged by ICAM-1 post pMHC-TCR interaction<sup>34</sup> (*right*); **(3)** Inflammation, which involves the conformational change of neutrophil LFA-1 upon impingement by intercellular adhesion molecule 1 (ICAM-1)<sup>35</sup> (*left*), and the interaction between neutrophil P-selectin glycoprotein ligand 1 (PSGL-1) and P-selectin<sup>21,36,37</sup> (*right*); and **(4)** Virology, which includes the investigation of the extension of severe acute respiratory syndrome coronavirus 2 (SARS-CoV-2) variants (alpha, beta, gamma, delta, and omicron) upon interaction with the angiotensin-converting enzyme 2 (ACE2) receptors<sup>3</sup>. The black arrows in the figure indicate the direction of the force of the molecular interaction.

## 2. Conventional BFP Technique

Initially, the conventional BFP was developed to measure strengths of single ligand-receptor bonds and receptor-membrane anchoring over an enormous range of loading rates from  $10^{-1}$  pN/s to  $10^5$  pN/s<sup>39</sup> with measurements at  $\sim 1$  pN,  $\sim 3$  nm, and  $\sim 0.5$  ms in force, spatial, and temporal resolution<sup>40</sup>. The brilliance of BFP is that it allows us to test the strength of bonds to determine the maximum force that a molecular attachment can support at the instant of failure.

As described above, conventional BFP uses a pre-swollen RBC (a naturally elastic biomaterial) as an ultrasensitive force transducer with a compatible spring constant range from 0.1-3 pN/nm<sup>40</sup>, which enables the measurement of single molecule 2-dimensional kinetics, mechanical properties, and conformational changes (Figure 2). Central to the BFP methodology is the determination of the spring constant<sup>13</sup>. Evans *et al.* have studied the deformation of an RBC submitted to a force and defined the erythrocyte behaviour at small deformation as a Hookean spring with a constant ( $k_{RBC}$ ):

$$k_{RBC} = \frac{\pi R_p \Delta p}{(1 - R_p/R_0) \ln[4R_0^2/R_p R_c]} \quad (1.1);$$

Where  $\Delta p$  is the aspiration pressure at probe pipette tip,  $R_0$ ,  $R_p$ , and  $R_c$  are the radii of the RBC, the probe micropipette inner orifice, and the circular contact area between the probe bead and the RBC, respectively<sup>9</sup> as demonstrated in Figure 2. Force ( $F$ ) is calculated using Hooke's law,

$$F = k_{RBC} \cdot \Delta x \quad (1.2);$$

Where  $k_{RBC}$  is the spring constant of the RBC and  $\Delta x$  is the displacement of the probe bead, which is tracked by a valley detection algorithm<sup>27</sup>. The target micropipette is then retracted and held with a clamped force while RBC is deformed by the ligand-receptor bond forces whose displacement is monitored in real-time by fast video imaging. Table 1 summarizes the key

mechanical parameters that can be manipulated with the conventional BFP setup—contact time (s), impingement force (pN), and ramping rate (pN/s). By analyzing the BFP force vs. time traces through the entire approaching, impinging, retracting, clamping, and bond dissociating test cycle, bond 2D kinetics (association  $k_{on}$  and dissociation  $k_{off}$ )<sup>32,41,42</sup>, bond lifetime<sup>24,43,44</sup>, molecular stiffness<sup>45</sup>, and intracellular events (with the aid of fluorescence microscopy)<sup>25,46,47</sup> can be obtained (Table 3).

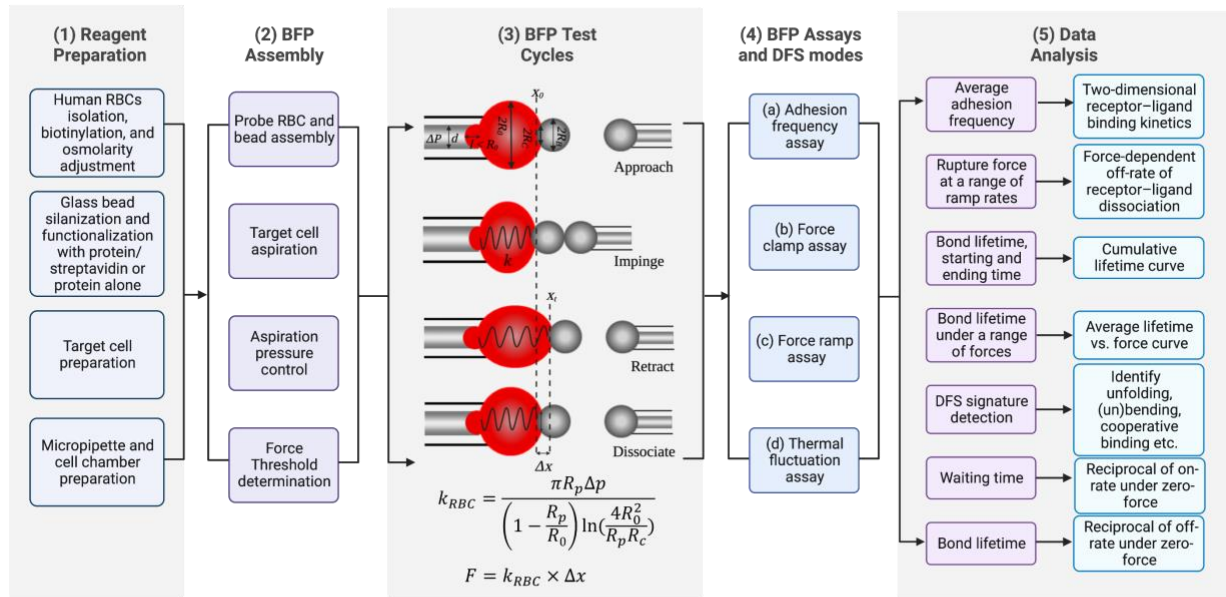


**Figure 2 Workflow of BFP dynamic force spectroscopies.** This flow chart illustrates the key steps in the biomembrane force probe (BFP) workflow. This process begins with (1) reagent preparation, followed by (2) BFP assembly, and then the execution of (3) BFP test cycles. These test cycles consist of four BFP assays and dynamic force spectroscopy (DFS) modes, which are (a) adhesion frequency, (b) force clamp, (c) force ramp, and (d) thermal fluctuation assays. Finally, the data generated during these assays are analyzed (5). The BFP test cycle (3) depicts the deflection of the red blood cell (RBC) and the position of the probe and target bead in a touch cycle. The target bead approaches and impinges the probe bead, then retracts. The vertical dashed lines indicate the zero-force position of the RBC apex. The variables involved in the BFP experiment include  $k_{RBC}$  (spring constant of the RBC),  $\Delta P$  (aspiration pressure applied to the probe pipette),  $R_p$  (pipette radius),  $R_0$  (RBC radius outside the pipette),  $R_c$  (radius of the contact area between the RBC and the bead),  $R_b$  (probe bead radius), and  $\Delta x$  (displacement of the probe bead and the deformation of the RBC). The radius of the RBC tail,  $l$ , should be comparable to  $R_0$ . The variables  $k_{RBC}$  and the binding force,  $F$ , can be quantified using these variables.

### 3. BFP Assays

#### 3.1 Adhesion Assay

Hereby, we would like to highlight key BFP assays and DFS modes, the first of which is the adhesion frequency assay. While this method was originally developed to be used in the context of micropipette aspiration in which a human RBC is used as an adhesion sensor, it can be modified and applied in the context of BFP. Briefly, the micropipette adhesion assay was developed by Chesla *et al.* to measure two-dimensional ligand-receptor binding kinetics and was based on the premise that adhesion probability depends on contact duration and densities of receptors and ligands<sup>48</sup>. From the time of its development, the assay has been validated using selectins with respective glycoconjugate ligands<sup>49–51</sup>, integrins with respective ligands<sup>35,52–54</sup>, T cell receptor and coreceptor (TCR) with peptide-major histocompatibility complexes (pMHC)<sup>19,55–58</sup>, and Fc gamma (Fc $\gamma$ ) receptors with immunoglobulin G (IgG) Fc<sup>48,49,59–62</sup>. In the micropipette aspiration assay, the RBC is coated with ligands of interest and directly brought into contact with another cell that expresses the opposing receptors with precisely controlled area and time to enable bond formation<sup>63</sup>. To achieve higher spatial and temporal resolution, this assay was modified in the context of BFP by attaching a glass bead to the apex of the RBC (Figure 2). Moreover, in cases where the off-rate is greater than 5 s<sup>-1</sup>, BFP is preferred. Meanwhile, the micropipette assay only detects binding events visually, so BFP has the benefit of implementing a high-speed camera and real-time tracking.

For example, Huang *et al.* utilized the BFP to perform an adhesion frequency assay, where a T cell was micro-manipulated to touch the opposing bead with a controlled contact area or for a controlled time<sup>19</sup>. Interest in the kinetic analysis of TCR and pMHC stems from the critical role of this interaction in determining immune response<sup>64</sup>. In this adhesion assay, the likelihood of adhesion was estimated from the frequency of adhesions ( $P_a$ ) observed in 50 repeated contact cycles using a single pair of beads/cells (Table 2).

$$P_a = 1 - \exp(-n) \quad (2.1);$$

Where  $P_a$  is the adhesion frequency, and

$$n = m_r m_l A_c K_a [1 - \exp(-k_{off} t_c)] \quad (2.2);$$

Where  $m_r$  and  $m_l$  are respective receptor (e.g., TCR) and ligand(e.g., pMHC) densities,  $A_c$  and  $t_c$  are contact area and time, and  $K_a$  and  $k_{off}$  are 2D binding affinity and off-rate. The 2D on rate can be calculated from  $k_{on} = K_a \times k_{off}$ . Since its advent, this BFP adhesion assay has been applied to other cell types, including platelets<sup>29,65</sup> and neutrophils<sup>15,66</sup>.

### 3.2 Thermal Fluctuation Assay

In addition to the adhesion frequency assay, the thermal fluctuation assay is also used to measure 2D binding kinetics of ligand-receptor pairs (Figure 2). While the adhesion frequency assay measures the binding frequency as a function of contact duration and extracts the 2D kinetic parameters by nonlinearly fitting the data with a probabilistic model, the thermal fluctuation assay detects bond formation and dissociation by monitoring the reduction and resumption of thermal fluctuations by a force sensor<sup>67</sup>. The premise of the thermal fluctuation assay is that force probes, such as BFP are usually susceptible to thermal fluctuations<sup>67</sup>. In fact, Chen and Evans first developed the method for monitoring 2D ligand-receptor interactions based solely on thermal fluctuations of the BFP probe<sup>50</sup>. They utilized the BFP to monitor the interactions between P-selectin glycoprotein ligand-1 (PSGL-1) coated on the probe glued to the apex of the RBC and L-selectin or P-selectin on the target bead.

### 3.3 Force-clamp DFS Assay

BFP can also be used to measure single ligand-receptor bond lifetimes under a range of constant forces. This assay is termed a force-clamp assay and has been utilized by several groups studying both platelets<sup>25-27,45</sup> and T cells<sup>33,46</sup>. In a recent paper, Chen *et al.* utilized the force-clamp assay to elucidate distinct state transitions of platelet integrin,  $\alpha_{IIb}\beta_3$ , during platelet aggregation<sup>45</sup>. Briefly, platelets play a key role in many physiological and pathological processes, and these responses are heavily mediated by integrin  $\alpha_{IIb}\beta_3$ <sup>68</sup>. In the assay, the probe bead was coated with fibronectin (FN) and the opposing platelet was driven to contact and impinge the probe bead and then retracted at a constant rate (3  $\mu\text{m/s}$ ). During retraction, if binding was detected, the target pipette was held at a set force to wait for bond dissociation.

Using platelets again, Ju *et al.* employed the BFP force-clamp assay and found that force can unfold multiple leucine-rich repeats (LRR) in glycoprotein Iba (GPIb $\alpha$ ) starting from the noncontact LRR2-4. The observed force-strengthened bond behavior, where forces in the range of 10-25 pN strengthened individual bonds between Von Willebrand factor-A1 domain (VWF-A1) and platelet receptor GPIb $\alpha$ , is consistent with their previous reports<sup>26,29,69</sup> suggesting the unfolding events allows for a better fit of the A1 domain into the enlarged GPIb $\alpha$  binding pocket thus prolongs the lifetime of the bond<sup>26</sup>, providing a potential explanation for platelet agglutination via VWF-GPIb $\alpha$  alone under pathological shear ( $>10,000 \text{ s}^{-1}$ )<sup>70</sup>. Furthermore, the GPIb $\alpha$  juxta membrane mechanosensitive domain (MSD) was demonstrated to unfold under force and trigger  $\alpha$ -type intracellular  $\text{Ca}^{2+}$  signalling, while LRRD unfolding intensified  $\text{Ca}^{2+}$

signals. Intriguingly, a cytoplasmic adaptor protein 14-3-3 $\zeta$  was found to function as a signal-transducer, where it transmits force on the VWF-GPIIb $\alpha$  bond (whose lifetime is prolonged by LRRD unfolding) to the MSD, which provides a coupling between the two unfolded domains<sup>25</sup> (Table 4).

### 3.4 Force-ramp DFS Assay

Another key assay performed using the BFP is the force-ramp assay (Figure 2). The force-ramp assay is used to detect the occurrence of adhesions at the end of a pre-set contact time for the adhesion frequency assay<sup>45</sup>. For example, Liu *et al.* utilized the force-ramp BFP assay with T cells. As such, a T cell was pulled at a constant speed until bond rupture.<sup>33</sup> In a novel approach, Evans *et al.* utilized two modes of force spectroscopy with the BFP force-ramp assay: a conventional “steady ramp” and a new “jump/ramp.” They found that force history can select between two pathways for dissociation with very different kinetics. Pulled with slow steady ramps, starting from zero force, P-selectin-PSGL-1 bonds are weak and break rapidly at very small forces, indicating a low impedance failure pathway with a fast dissociation rate. By comparison, when pulled in the same way under fast force ramping rates, P selectin-PSGL-1 bonds become strong and break at forces rising in proportion to the logarithm of the loading rate, demonstrating a high impedance failure pathway even if pulled very slowly. Labelled as a “catch-slip” bond, it was shown that pulling with a relatively small force can first strengthen a bond, extending its lifetime. Subsequently, exposing the bond to higher forces can then lower the principal energy barrier to speed up failure of the bond<sup>71</sup> (Table 4).

### 3.5 Multimode Assays

Ultimately, the BFP is a highly versatile tool, that can be utilized in an array of contexts. Table 3 illustrates key events that can be monitored with a combination of the BFP assays described in this review. Combining several of the assays described above, Ju *et al.* observed biphasic force decelerated (catch) and force accelerated (slip) dissociation of GPIIb $\alpha$  from VWF on platelets<sup>29</sup> (Table 4), confirming previous experiments demonstrating this catch-slip phenomenon<sup>69</sup>. Used as an in house set up with custom written LabVIEW programs for image analysis and piezo electric translator control, they ran repeat impingement cycles to measure adhesion frequency and bond lifetime (force-clamp assay at nonzero forces and thermal fluctuation assay at zero force)<sup>29</sup>.

Additionally, using a combination of force-clamp and thermal fluctuation experiments, Chen *et al.* showed intercellular adhesion molecule 1 (ICAM-1) binding to lymphocyte

function-associated antigen 1 (LFA-1) at different conformations, including the bent conformation with the lowest affinity state. They quantified how force and conformations of LFA-1 regulate its kinetics with ICAM-1 (Table 4). Three states with distinct off-rates were identified from lifetime distributions. Force shifted the associated fractions from the short to intermediate and long-lived states, producing catch bonds at low forces, but increased their off rates exponentially, converting catch to slip bonds at high forces<sup>72</sup>. Similarly, thermal fluctuation and force-clamp experiments were used to quantify how initial and subsequent conformations of LFA-1 regulate the force-dependent kinetics of dissociation from ICAM-1, providing new insights into how integrins function to precisely control cell adhesion and signalling<sup>73</sup>.

Finally, TCR on T cells recognize pMHC complexes on antigen-presenting cells to initiate T cell signalling and adaptive immunity. Wu *et al.* used the thermal fluctuation and adhesion frequency assays on the BFP to test whether these force-enhanced or force-induced H-bonds at the pMHC-TCR binding interface could affect pMHC-TCR catch bonds (Table 4). The relationship between human leukocyte antigens (HLAs) and cancer has been intensively investigated, and cancer-associated somatic mutations in HLA-A2 have been identified. They demonstrated that mechanical force induced dynamic mechano-chemical coupling sequentially changed agonist pMHC conformations. Significantly, this was essential for the activation of both mouse and human pMHC-TCR catch bonds, amplification of TCR antigen discrimination and initiation of T cell functions. Finally, restriction of pMHC conformational changes by cancer-associated somatic mutations, suppressed pMHC-TCR catch bonds<sup>74</sup>.

## **4. BFP Upgrades**

### **4.1 Dual BFP (dBFP)**

Next, we would like to detail two key BFP upgrades, the first of which is the development of a dual BFP system (dBFP), represented in Table 5. Ju *et al.* developed the dBFP system, which uses two probe- and two target-micropipettes and enables the analysis of dual receptor crosstalk on a single cell in a step-by-step manner<sup>77</sup>. The signal initiated upon one receptor binding will travel over a distance to activate the other receptor. Temporal crosstalk involves presenting two ligands by two separate probes at distinct time points, allowing the signal initiated upon the first ligand-receptor binding event to upregulate another receptor. The power and utility of this dBFP was nicely demonstrated in four important dual receptor systems:

(TCR/LFA-1), (GPIIb $\alpha$ / $\alpha$ IIb $\beta$ 3), (GPIIb $\alpha$ /CD62p), and (P<sub>2</sub>Y<sub>1</sub>/CD62p)<sup>27</sup>. The dBFP is like the conventional BFP, configured with four micropipettes instead of three.

For example, Pang *et al.* utilized a modified dBFP method to primarily stimulate integrin  $\alpha$ IIb $\beta$ 3 and subsequently report phosphatidylserine (PS) exposure<sup>77</sup>. In this study, the stimulating BFP probe was coated with FN and the test micropipette with the platelet was first brought into repeated contact and retraction with the FN beads for a period of 5 minutes. Then the position of the platelet was quickly realigned from the stimulating micropipette to the reporting micropipette for measurement of annexin V binding to report PS exposure. This new technology allowed Pang *et al.* to correlate platelet activation, specifically activation of integrin  $\alpha$ IIb $\beta$ 3, with PS exposure. A few years later, Chen *et al.* also utilized the new dBFP technology to switch a platelet from a VWF-A1 probe to a FN or fibrinogen (FBG) probe to measure the integrin  $\alpha$ IIb $\beta$ 3 adhesion frequency after the first VWF-A1-GPIIb $\alpha$  lifetime event regardless of its duration<sup>45</sup>. As a result, they found that the post-switch adhesion frequency of integrin  $\alpha$ IIb $\beta$ 3 was found to increase with the A1 lifetime, indicating a mechanical dose dependency of integrin  $\alpha$ IIb $\beta$ 3 activation, supporting its role in arresting platelet from translocation under high shear<sup>78,79</sup> (Table 5). Ultimately, this novel upgrade in BFP enables the quantification of the spatiotemporal requirements and reveals the functional consequences of the up-and down-stream signalling events<sup>8</sup>.

#### **4.2 Fluorescence BFP (fBFP)**

Another influential BFP technical advancement was the development of fluorescence BFP (fBFP) described in detail by Chen *et al.*<sup>65</sup> and is represented in Table 6. When combined with fluorescence imaging, BFP-DFS directly correlates the force experienced on a cell with ligand-receptor binding kinetics and subsequent intracellular calcium signalling. For example, Chen *et al.* used the fBFP system in combination with microfluidics and cone-and-plate rheometry to precisely control mechanical stimulations of platelets to elucidate intermediate conformations of integrin  $\alpha$ IIb $\beta$ 3. Notably, fBFP was instrumental in showing distinctive intraplatelet Ca<sup>2+</sup> patterns in stimulated and unstimulated platelets, contributing to the characterization of the integrin  $\alpha$ IIb $\beta$ 3<sup>45</sup>. Additionally, Ju *et al.* combined the fBFP with their novel dBFP setup to monitor Ca<sup>2+</sup> signalling in platelets upon GPIIb $\alpha$  activation<sup>27</sup>. Remarkably, they were able to directly correlate Ca<sup>2+</sup> signalling with binding events and bond lifetimes on single platelets during GPIIb $\alpha$  activation. Further, fBFP was also utilized to monitor adenosine

diphosphate (ADP) binding to P<sub>2</sub>Y receptors on platelets and track platelet activation through Ca<sup>2+</sup> increases<sup>27</sup>.

Similarly, Liu *et al.* utilized the force-clamp BFP assay with T cells in conjunction with fBFP<sup>33</sup>. In this study, 2D single bond lifetimes under a range of constant forces were applied via a pMHC engaged to a TCR on a naive T cell from OT1 transgenic mice. Bond lifetimes were measured by a force-clamp assay in repetitive cycles. Contact was brief (0.1s) to minimize multiband formation. To ensure that most binding events were mediated by single bonds, adhesion frequencies were kept low (<20%) by adjusting the pMHC density on the probe bead. Interestingly, fBFP was used simultaneously to measure bond lifetime and Ca<sup>2+</sup> flux. Further, to examine how various attributes of force impact T cell triggering, force was correlated with maximal percent of Ca<sup>2+</sup> increase<sup>33</sup>. In summary, coupling of fluorescence imaging with the conventional BFP setup has provided researchers with the ability to monitor membrane ligand-receptor interaction and cellular signalling simultaneously (Table 6).

## 5. BFP Applications

### 5.1 Immunology

The mechanical insights gleaned from BFP have cumulatively contributed to the field of cancer biology (Table 7). Recently, An *et al.* utilized BFP to benchmark the dissociation kinetics of three clinically approved monoclonal antibodies (mAbs) that target programmed cell death protein (PD-1) on T lymphocytes. They developed an ultra-stable BFP force-clamp assay to measure long bond lifetimes beyond 200 s with stably and accurately clamped holding forces. In doing so, they were able to precisely characterize mAb-immunotherapeutic target binding kinetics at the single molecule level, suggesting a kinetic platform to direct the screening, optimization, and clinical selection of therapeutic antibodies in the future<sup>41</sup>. Another group recently used BFP to characterize the conformational dynamics and binding kinetics of human integrin  $\alpha_v\beta_3$  expressed on mouse lung endothelial cells<sup>85</sup>. Integrin  $\alpha_v\beta_3$  has been shown to play a role in tumour metastasis and phagocytosis and understanding how its physiological function and molecular structure are coupled may translate clinically in the future. Similarly, other groups have implemented fBFP technology to gain insight into the nature of the forces exerted on T cells during antigen recognition and activation, which is crucial in the development of adaptive immunity in response to pathogens or tumor cells<sup>46</sup>. Utilizing the novel fBFP, Husson *et al.* were able to simultaneously image cell morphology and Ca<sup>2+</sup> signalling through fluorescent imaging. In a more recent, but similar study, Liu *et al.* also

utilized fBFP to observe  $\text{Ca}^{2+}$  signals induced by force in live T cells<sup>47</sup>. Finally, using a modified BFP method, Sawicka *et al.* revealed changes in Young's modulus of T cells during their activation, demonstrating a cellular stiffening effect within the first minutes of the activation process<sup>86</sup>.

## 5.2 Thrombosis

Furthermore, BFP has also been influential in the field of thrombosis to characterize the kinetics of platelet receptors involved in the exaggerated haemostatic response (Table 7). One key platelet receptor studied quite extensively using BFP is GPIIb/IIIa. Ju *et al.* showed that GPIIb/IIIa conformational changes enhance binding to VWF-A1<sup>26</sup>. Similarly, BFP was used extensively to demonstrate the role of force transduction on platelet surface reactivity<sup>25</sup>. Additionally, BFP was used to characterize the force-dependent kinetics of GPIIb/IIIa dissociation from the VWF-A1 domain of different N-terminal lengths immobilized on different surfaces. Ultimately, these findings helped to explain the four phases of collagen-dependent enhancement of VWF–GPIIb/IIIa interaction under flow, providing novel insight into platelet dynamics during thrombotic response<sup>30</sup>. Moreover, BFP has been used to explain the mechanobiology of another key platelet receptor: integrin  $\alpha_{\text{IIb}}\beta_3$ . Interestingly, Xu *et al.* employed BFP to detect direct interactions between apolipoprotein A-IV (apoA-IV), which is an abundant plasma lipid binding protein inversely correlated with cardiovascular disease, and integrin  $\alpha_{\text{IIb}}\beta_3$ . Through their work, they identified apoA-IV as an endogenous inhibitor of thrombosis<sup>28</sup>. More recently, studies have demonstrated the existence of a compression force sensing mechanism linked to  $\alpha_{\text{IIb}}\beta_3$  adhesive function that leads to a distinct prothrombotic phenotype in diabetes. Historically, it has been established that platelets from individuals with diabetes are more reactive than those from nondiabetics. BFP studies have attributed this increased reactivity in part to  $\alpha_{\text{IIb}}\beta_3$  dysregulated compression force sensing in diabetic patients<sup>80</sup>. In combination with other methodologies, BFP technology has been instrumental in showing distinct state transitions for  $\alpha_{\text{IIb}}\beta_3$  in response to biomechanical and biochemical stimuli, which identifies a role for the integrin intermediate state in promoting biomechanical platelet aggregation<sup>45</sup>.

## 5.3 Inflammation

Finally, BFP has provided molecular insight which has progressed our knowledge of the inflammatory response<sup>87</sup>. Evans *et al.* have worked extensively on utilizing BFP to understand neutrophil mechanobiology at the ligand-receptor scale. A series of articles published by Evans' group characterized and quantified the bond kinetics of PSGL-1 and P-selectin, which

are essential for neutrophil recruitment to the endothelium and play an important role in the immune response<sup>20,21,37</sup>. Briefly, this series of studies probed neutrophils with P-selectin coated probe beads and quantified the forces experienced by the attachment during the retraction of the neutrophils, providing valuable insight into neutrophil recruitment dynamics. Additionally, BFP has been used to investigate another key neutrophil receptor: LFA-1. Integrins are thought to be capable of not only transmitting forces, but also transducing signals bidirectionally across the cell membrane, thereby playing a key role in mechanosensing and mechanotransduction. BFP has revealed catch bond kinetics for ICAM-1-LFA-1 binding<sup>44</sup>, and the influence of both outside-in and inside-out signalling on ICAM-1-LFA-1 bond lifetimes<sup>15,16</sup>. Finally, in combination with a flow chamber, BFP was used to explain a triphasic force dependent of E-selectin–PSGL-1 dissociation on rolling neutrophils<sup>14</sup>. Overall, these molecular insights have helped to elucidate neutrophil tethering, rolling, and subsequent adhesion on vascular surfaces, which has widespread implications in the context of inflammation.

## 6. Future Perspectives

Overall, BFP has proven to be an immensely powerful technique to study cell mechanobiology *in vitro*. This technique has evolved significantly since its establishment only a few decades ago. What started as a simultaneous force probe and imaging modality has developed to now encompass fluorescent imaging and expanded to allow for dual receptor crosstalk investigation. In comparison to other DFS nanotools available, BFP offers benefits in force resolution and its compatibility with live cells. While positional resolution with BFP is 10x lower than that attainable with AFM, force resolution is significantly higher with a detection of ~3 pN at ~30 nanometer spatial resolution. In contrast to AFM, which is typically performed on cells adherent to a coverslip or cantilever surface, BFP is comprised of a micropipette in a buffer-filled chamber which gently holds cells in a nearly physiological environment<sup>88</sup>. Further, in contrast to techniques such as micropipette aspiration and AFM indentation which induce deformations by applying surface forces to the cell in a non-discriminatory manner, using ligand-coated micrometer sized beads allows the mechanical loads to be selectively applied to intracellular structures via specific receptors<sup>89</sup>.

### 6.1 Limitations

Nevertheless, challenges and limitations still exist in the applications of the BFP. While the BFP offers high sub-piconewton force resolution with an adjustable loading rate, a nanometer-

scale spatial resolution, and good temporal control with milliseconds resolution, it has relatively low throughput<sup>90</sup>. Additionally, it is time- and cost- intensive as only one pair of ligand-receptor interactions can be characterized at a given time. The measurements with the BFP are limited to pulling forces and displacements smaller than  $\sim 0.3 \mu\text{m}$ <sup>86</sup> and the cell of interest aspirated by the micropipette may experience a change in shape over time<sup>90</sup>.

## 6.2 Developments in DFS

The continued development and implementation of mechanical molecular nanotools combined with optical techniques have steadily advanced knowledge in single cell biomechanics. Nevertheless, there is a variation in these nanotool's throughput, sensitivities, and spatiotemporal resolutions, as well as an emerging need for characterizing and visualizing cell mechanosensing<sup>91</sup>. Additional advances in DFS have begun to integrate force spectroscopies with microfluidic systems to create a lab-on-a-chip platform to simulate the multicellular microenvironment of human-specific physiology and pathophysiology. For example, the OT-integrated microfluidic system has demonstrated its ability in sorting and/or manipulating biological molecules<sup>92–94</sup>. More importantly, a microfluidic-integrated micro clot-array-elastometry system has recapitulated the dynamics of platelet clot biomechanics under haemodynamic shear force and biochemical treatments<sup>95</sup>, highlighting its potential in identifying therapeutic targets, translating into a point-of-care system for coagulation diagnosis and a high-throughput antiplatelet drug testing platform. On the other hand, to improve the throughput of micropipette-based techniques such as BFP, an automated operational procedure for using parallel arrays of serial micropipettes on a microfluidic platform has been established<sup>96,97</sup>. This parallel setup has demonstrated the ability to capture multiple dynamic measurements of individual cells simultaneously, where each cell is sampled multiple times by the serial micropipettes to assess consequential effects. Therefore, parallelization enables the user to appreciate cell dynamics and variability and offers higher throughput for laboratory research and potential clinical drug testing and screening.

Force spectroscopy traces are often acquired at a high acquisition rate to capture dwells in transient dynamics and short-lived molecular states. However, the slow response of the single molecule force spectroscopy can distort the signal and lead to misinterpretation of results by data-processing algorithms<sup>98</sup>. To address these response dynamics, an adaptation of Bayesian nonparametric computational algorithm offers high potential. It allows for clear physical interpretation and provides posterior probabilities for modelling complex biomolecules<sup>99</sup>. The

algorithm was established to allow data acquired within the low kHz timeframe to be analyzed, and presents a clear interpretation of molecular dynamic transitions, instrumentation response, and noise<sup>98</sup> Further, this adapted algorithm sees a potential for unsupervised time series analysis of cell adhesion and spreading when combined with single-molecule force microscopies<sup>98</sup> such as super-resolution microscopy<sup>100</sup>.

## 7. Conclusion

Biomembrane force probe is a precise nanotool for investigating molecular interactions and cell mechanosensing. It has potential applications in cancer, thrombosis, inflammation, and drug targeting. However, the niche technology's accessibility to many laboratories remains a challenge. Developing user-friendly data processing interfaces and automating the tool can improve its feasibility. Stable feedback control algorithms can improve the BFP's force resolution, an essential factor in expanding its potential applications. Recent developments, such as the "BFPTool," have integrated and simplified BFP experiment image processing and analysis, making it more accessible to researchers<sup>101</sup>. BFP has also shown potential in clinical applications, elucidating monoclonal antibodies' dissociation kinetics<sup>41</sup>, platelet receptor kinetics for potential drug targeting<sup>26,27,30,80</sup>, and neutrophil recruitment in inflammation<sup>21,37</sup>. With the growing interest in the field of cell mechanobiology, BFP is expected to continue expanding as a cutting-edge technology for studying biology at the single-cell level. By improving user-friendliness and clinical relevance, BFP technology can advance our understanding of cellular mechanics and contribute to novel therapeutic discoveries. The development of stable feedback control algorithms<sup>41</sup>, automation, and user-friendly data processing interfaces can increase its output and efficiency<sup>46,102</sup>.

## Acknowledgments

We thank Shaun Jackson and Thrombosis Group at Heart Research Institute for human resources support. This work was supported by the Australian Research Council (ARC) (DP200101970 – L.A.J.); the National Health and Medical Research Council (NHMRC) of Australia (APP2003904 – L.A.J.); NSW Cardiovascular Capacity Building Program (Early-Mid Career Researcher Grant – L.A.J.); Office of Global and Research Engagement (International Sustainable Development Goal Program – L.A.J.), and Sydney Nano Research Schemes (Grand Challenge – L.A.J.). L.A.J. is an National Heart Foundation Future Leader Fellow Level 2 (105863

## Author Contributions

L.M., C.H.S., and C.Y.C. contributed equally to the preparation of this manuscript. L.M. and C.H.S. co-wrote the manuscript. C.H.S. C.Y.C. and L.M. prepared the figures and tables. J.H.W. provided key comments to this manuscript. L.A.J. supervised and co-wrote this manuscript.

## References

- (1) Krieg, M.; Fläschner, G.; Alsteens, D.; Gaub, B. M.; Roos, W. H.; Wuite, G. J. L.; Gaub, H. E.; Gerber, C.; Dufrêne, Y. F.; Müller, D. J. Atomic Force Microscopy-Based Mechanobiology. *Nature Reviews Physics*. Springer Nature January 1, 2019, pp 41–57. <https://doi.org/10.1038/s42254-018-0001-7>.
- (2) Kim, D. H.; Pak, K. W.; Park, J.; Levchenko, A.; Sun, Y. Microengineered Platforms for Cell Mechanobiology. *Annual Review of Biomedical Engineering*. August 2009, pp 203–233. <https://doi.org/10.1146/annurev-bioeng-061008-124915>.
- (3) Hu, W.; Zhang, Y.; Fei, P.; Zhang, T.; Yao, D.; Gao, Y.; Liu, J.; Chen, H.; Lu, Q.; Mudianto, T.; Zhang, X.; Xiao, C.; Ye, Y.; Sun, Q.; Zhang, J.; Xie, Q.; Wang, P.-H.; Wang, J.; Li, Z.; Lou, J.; Chen, W. Mechanical Activation of Spike Fosters SARS-CoV-2 Viral Infection. *Cell Res* **2021**, *31* (10), 1047–1060. <https://doi.org/10.1038/s41422-021-00558-x>.
- (4) Clausen-Schaumann, H.; Seitz, M.; Krautbauer, R.; Gaub, H. E. Force Spectroscopy with Single Bio-Molecules. *Curr Opin Chem Biol* **2000**, *4* (5), 524–530. [https://doi.org/https://doi.org/10.1016/S1367-5931\(00\)00126-5](https://doi.org/https://doi.org/10.1016/S1367-5931(00)00126-5).
- (5) Evans, E.; Williams, P. Dynamic Force Spectroscopy. In *Physics of bio-molecules and cells. Physique des biomolécules et des cellules*; Flyvbjerg, F., Jülicher, F., Ormos, P., David, F., Eds.; Springer Berlin Heidelberg: Berlin, Heidelberg, 2002; pp 145–204.
- (6) Evans, E.; Ritchie, K.; Merkel, R. *Sensitive Force Technique to Probe Molecular Adhesion and Structural Linkages at Biological Interfaces*; 1995; Vol. 68.
- (7) Wang, H.; Zhou, F.; Guo, Y.; Ju, L. A. Micropipette-Based Biomechanical Nanotools on Living Cells. *European Biophysics Journal*. Springer Science and Business Media Deutschland GmbH March 1, 2022, pp 119–133. <https://doi.org/10.1007/s00249-021-01587-5>.
- (8) Su, Q. P.; Ju, L. A. Biophysical Nanotools for Single-Molecule Dynamics. *Biophysical Reviews*. Springer Verlag October 1, 2018, pp 1349–1357. <https://doi.org/10.1007/s12551-018-0447-y>.
- (9) Gourier, C.; Jegou, A.; Husson, J.; Pincet, F. A Nanospring Named Erythrocyte. The Biomembrane Force Probe. *Cell Mol Bioeng* **2008**, *1* (4), 263–275. <https://doi.org/10.1007/s12195-008-0030-x>.
- (10) Lou, J.; Yago, T.; Klopocki, A. G.; Mehta, P.; Chen, W.; Zarnitsyna, V. I.; Bovin, N. v; Zhu, C.; McEver, R. P. Flow-Enhanced Adhesion Regulated by a Selectin Interdomain Hinge. *Journal of Cell Biology* **2006**, *174* (7), 1107–1117. <https://doi.org/10.1083/jcb.200606056>.
- (11) Min, S.; Hui, C.; Qinghua, J.; Jianhui, X.; Yanzhe, H.; Jizhong, L. Measuring the Elasticity of Liquid–Liquid Phase Separation Droplets with Biomembrane Force Probe. *Biophys Rep* **2022**, *8* (2), 68–79. <https://doi.org/10.52601/bpr.2022.210038>.

- (12) Evans, E.; Leung, A.; Heinrich, V.; Zhu, C. Mechanical Switching and Coupling between Two Dissociation Pathways in a P-Selectin Adhesion Bond. *Proc Natl Acad Sci U S A* **2004**, *101* (31), 11281–11286. <https://doi.org/10.1073/pnas.0401870101>.
- (13) Merkel, R.; Nassoy, P.; Leung, A.; Ritchie, K.; Evans, E. Energy Landscapes of Receptor–Ligand Bonds Explored with Dynamic Force Spectroscopy. *Nature* **1999**, *397* (6714), 50–53. <https://doi.org/10.1038/16219>.
- (14) Wayman, A. M.; Chen, W.; McEver, R. P.; Zhu, C. Triphasic Force Dependence of E-Selectin/Ligand Dissociation Governs Cell Rolling under Flow. *Biophys J* **2010**, *99* (4), 1166–1174. <https://doi.org/10.1016/j.bpj.2010.05.040>.
- (15) Evans, E.; Kinoshita, K.; Simon, S.; Leung, A. Long-Lived, High-Strength States of ICAM-1 Bonds to B2 Integrin, I: Lifetimes of Bonds to Recombinant AL B2 under Force. *Biophys J* **2010**, *98* (8), 1458–1466. <https://doi.org/10.1016/j.bpj.2009.09.067>.
- (16) Kinoshita, K.; Leung, A.; Simon, S.; Evans, E. Long-Lived, High-Strength States of ICAM-1 Bonds to B2 Integrin, II: Lifetimes of LFA-1 Bonds under Force in Leukocyte Signaling. *Biophys J* **2010**, *98* (8), 1467–1475. <https://doi.org/10.1016/j.bpj.2009.12.4316>.
- (17) Zhao, Y. C.; Wang, H.; Wang, Y.; Lou, J.; Ju, L. A. The N-Terminal Autoinhibitory Module of the A1 Domain in von Willebrand Factor Stabilizes the Mechanosensor Catch Bond. *RSC Chem Biol* **2022**, *3* (6), 707–720. <https://doi.org/10.1039/d2cb00010e>.
- (18) Ju, L.; Qian, J.; Zhu, C. Transport Regulation of Two-Dimensional Receptor-Ligand Association. *Biophys J* **2015**, *108* (7), 1773–1784. <https://doi.org/https://doi.org/10.1016/j.bpj.2015.02.023>.
- (19) Huang, J.; Zarnitsyna, V. I.; Liu, B.; Edwards, L. J.; Jiang, N.; Evavold, B. D.; Zhu, C. The Kinetics of Two-Dimensional TCR and PMHC Interactions Determine T-Cell Responsiveness. *Nature* **2010**, *464* (7290), 932–936. <https://doi.org/10.1038/nature08944>.
- (20) Heinrich, V.; Leung, A.; Evans, E. Nano- to Microscale Dynamics of p-Selectin Detachment from Leukocyte Interfaces. II. Tether Flow Terminated by p-Selectin Dissociation from PSGL-1. *Biophys J* **2005**, *88* (3), 2299–2308. <https://doi.org/10.1529/biophysj.104.051706>.
- (21) Evans, E.; Heinrich, V.; Leung, A.; Kinoshita, K. Nano- to Microscale Dynamics of P-Selectin Detachment from Leukocyte Interfaces. I. Membrane Separation from the Cytoskeleton. *Biophys J* **2005**, *88* (3), 2288–2298. <https://doi.org/10.1529/biophysj.104.051698>.
- (22) King, M. R.; Heinrich, V.; Evans, E.; Hammer, D. A. Nano-to-Micro Scale Dynamics of P-Selectin Detachment from Leukocyte Interfaces. III. Numerical Simulation of Tethering under Flow. *Biophys J* **2005**, *88* (3), 1676–1683. <https://doi.org/10.1529/biophysj.104.051805>.
- (23) Li, Z.; Lin, J.; Sulchek, T.; Cruz, M. A.; Wu, J.; Dong, J. fei; Zhu, C. Domain-Specific Mechanical Modulation of VWF–ADAMTS13 Interaction. *Mol Biol Cell* **2019**, *30* (16), 1920–1929. <https://doi.org/10.1091/mbc.E19-01-0021>.
- (24) Fiore, V. F.; Ju, L.; Chen, Y.; Zhu, C.; Barker, T. H. Dynamic Catch of a Thy-1-A5 B1 +syndecan-4 Trimolecular Complex. *Nat Commun* **2014**, *5*. <https://doi.org/10.1038/ncomms5886>.
- (25) Ju, L.; Chen, Y.; Xue, L.; Du, X.; Zhu, C. Cooperative Unfolding of Distinctive Mechanoreceptor Domains Transduces Force into Signals. **2016**. <https://doi.org/10.7554/eLife.15447.001>.
- (26) Ju, L.; Lou, J.; Chen, Y.; Li, Z.; Zhu, C. Force-Induced Unfolding of Leucine-Rich Repeats of Glycoprotein Iba Strengthens Ligand Interaction. *Biophys J* **2015**, *109* (9), 1781–1784. <https://doi.org/10.1016/j.bpj.2015.08.050>.
- (27) Ju, L.; Chen, Y.; Li, K.; Yuan, Z.; Liu, B.; Jackson, S. P.; Zhu, C. Dual Biomembrane Force Probe Enables Single-Cell Mechanical Analysis of Signal Crosstalk between Multiple Molecular Species. *Sci Rep* **2017**, *7* (1). <https://doi.org/10.1038/s41598-017-13793-3>.

- (28) Xu, X.; Spring, C. M.; Ju, L.; Wang, Y.; Rehemian, A.; Yang, H.; Jin, J. W.; Lei, X.; Yang, Y.; Reddy, E. C.; Chen, Y.; Chen, P.; Zhu, G.; Marchese, P.; Zarpellon, A.; Zhang, H.; She, Y.; Cyr, T.; Zhu, C.; Freedman, J.; Tso, P.; Davidson, S.; Ruggeri, Z. M.; Ni, H. Apolipoprotein A-IV Is a Novel Ligand of Platelet  $\text{Alb}\beta 3$  Integrin and an Endogenous Thrombosis Inhibitor: Measurement of Single-Molecular Interactions By Biomembrane Force Probe. *Blood* **2014**, *124* (21), 92–92. <https://doi.org/10.1182/blood.v124.21.92.92>.
- (29) Ju, L.; Dong, J. F.; Cruz, M. A.; Zhu, C. The N-Terminal Flanking Region of the A1 Domain Regulates the Force-Dependent Binding of von Willebrand Factor to Platelet Glycoprotein Iba. *Journal of Biological Chemistry* **2013**, *288* (45), 32289–32301. <https://doi.org/10.1074/jbc.M113.504001>.
- (30) Ju, L.; Chen, Y.; Zhou, F.; Lu, H.; Cruz, M. A.; Zhu, C. Von Willebrand Factor-A1 Domain Binds Platelet Glycoprotein Iba in Multiple States with Distinctive Force-Dependent Dissociation Kinetics. *Thromb Res* **2015**, *136* (3), 606–612. <https://doi.org/10.1016/j.thromres.2015.06.019>.
- (31) Chen, Y.; Ju, L. A.; Zhou, F.; Liao, J.; Xue, L.; Su, Q. P.; Jin, D.; Yuan, Y.; Lu, H.; Jackson, S. P.; Zhu, C. An Integrin  $\text{Alb}\beta 3$  Intermediate Affinity State Mediates Biomechanical Platelet Aggregation. *Nat Mater* **2019**, *18* (7), 760–769. <https://doi.org/10.1038/s41563-019-0323-6>.
- (32) Xu, X. R.; Wang, Y.; Adili, R.; Ju, L.; Spring, C. M.; Jin, J. W.; Yang, H.; Neves, M. A. D.; Chen, P.; Yang, Y.; Lei, X.; Chen, Y.; Gallant, R. C.; Xu, M.; Zhang, H.; Song, J.; Ke, P.; Zhang, D.; Carrim, N.; Yu, S. Y.; Zhu, G.; She, Y. M.; Cyr, T.; Fu, W.; Liu, G.; Connelly, P. W.; Rand, M. L.; Adeli, K.; Freedman, J.; Lee, J. E.; Tso, P.; Marchese, P.; Davidson, W. S.; Jackson, S. P.; Zhu, C.; Ruggeri, Z. M.; Ni, H. Apolipoprotein A-IV Binds  $\text{Alb}\beta 3$  Integrin and Inhibits Thrombosis. *Nat Commun* **2018**, *9* (1). <https://doi.org/10.1038/s41467-018-05806-0>.
- (33) Liu, B.; Chen, W.; Evavold, B. D.; Zhu, C. Accumulation of Dynamic Catch Bonds between TCR and Agonist Peptide-MHC Triggers T Cell Signaling. *Cell* **2014**, *157* (2), 357–368. <https://doi.org/https://doi.org/10.1016/j.cell.2014.02.053>.
- (34) Zhu, C.; Jiang, N.; Huang, J.; Zarnitsyna, V. I.; Evavold, B. D. Insights from in Situ Analysis of TCR–PMHC Recognition: Response of an Interaction Network. *Immunol Rev* **2013**, *251* (1), 49–64. <https://doi.org/https://doi.org/10.1111/imr.12016>.
- (35) Chen, W.; Lou, J.; Zhu, C. Forcing Switch from Short- to Intermediate- and Long-Lived States of the AA Domain Generates LFA-1/ICAM-1 Catch Bonds\*. *Journal of Biological Chemistry* **2010**, *285* (46), 35967–35978. <https://doi.org/https://doi.org/10.1074/jbc.M110.155770>.
- (36) Heinrich, V.; Leung, A.; Evans, E. Nano- to Microscale Dynamics of P-Selectin Detachment from Leukocyte Interfaces. II. Tether Flow Terminated by P-Selectin Dissociation from PSGL-1. *Biophys J* **2005**, *88* (3), 2299–2308. <https://doi.org/10.1529/BIOPHYSJ.104.051706>.
- (37) King, M. R.; Heinrich, V.; Evans, E.; Hammer, D. A. Nano-to-Micro Scale Dynamics of P-Selectin Detachment from Leukocyte Interfaces. III. Numerical Simulation of Tethering under Flow. *Biophys J* **2005**, *88* (3), 1676–1683. <https://doi.org/10.1529/biophysj.104.051805>.
- (38) Llorente García, I.; Marsh, M. A Biophysical Perspective on Receptor-Mediated Virus Entry with a Focus on HIV. *Biochimica et Biophysica Acta (BBA) - Biomembranes* **2020**, *1862* (6), 183158. <https://doi.org/https://doi.org/10.1016/j.bbamem.2019.183158>.
- (39) Evans, E. *Looking inside Molecular Bonds at Biological Interfaces with Dynamic Force Spectroscopy*; 1999; Vol. 82.
- (40) Obeidy, P.; Wang, H.; Du, M.; Hu, H.; Zhou, F.; Zhou, H.; Huang, H.; Zhao, Y. C.; Ju, L. A. Molecular Spring Constant Analysis by Biomembrane Force Probe Spectroscopy. *Journal of Visualized Experiments* **2021**, *2021* (177). <https://doi.org/10.3791/62490>.

- (41) An, C.; Hu, W.; Gao, J.; Ju, B. F.; Obeidy, P.; Zhao, Y. C.; Tu, X.; Fang, W.; Ju, L. A.; Chen, W. Ultra-Stable Biomembrane Force Probe for Accurately Determining Slow Dissociation Kinetics of PD-1 Blockade Antibodies on Single Living Cells. *Nano Lett* **2020**, *20* (7), 5133–5140. <https://doi.org/10.1021/acs.nanolett.0c01360>.
- (42) Chen, W.; Zarnitsyna, V. I.; Sarangapani, K. K.; Huang, J.; Zhu, C. Measuring Receptor–Ligand Binding Kinetics on Cell Surfaces: From Adhesion Frequency to Thermal Fluctuation Methods. *Cell Mol Bioeng* **2008**, *1* (4), 276–288. <https://doi.org/10.1007/s12195-008-0024-8>.
- (43) Ju, L.; Dong, J. F.; Cruz, M. A.; Zhu, C. The N-Terminal Flanking Region of the A1 Domain Regulates the Force-Dependent Binding of von Willebrand Factor to Platelet Glycoprotein Iba. *Journal of Biological Chemistry* **2013**, *288* (45), 32289–32301. <https://doi.org/10.1074/jbc.M113.504001>.
- (44) Chen, W.; Lou, J.; Zhu, C. Forcing Switch from Short- to Intermediate- and Long-Lived States of the AA Domain Generates LFA-1/ICAM-1 Catch Bonds. *Journal of Biological Chemistry* **2010**, *285* (46), 35967–35978. <https://doi.org/10.1074/jbc.M110.155770>.
- (45) Chen, Y.; Ju, L. A.; Zhou, F.; Liao, J.; Xue, L.; Su, Q. P.; Jin, D.; Yuan, Y.; Lu, H.; Jackson, S. P.; Zhu, C. An Integrin  $\text{AIIb}\beta 3$  Intermediate Affinity State Mediates Biomechanical Platelet Aggregation. *Nat Mater* **2019**, *18* (7), 760–769. <https://doi.org/10.1038/s41563-019-0323-6>.
- (46) Husson, J.; Chemin, K.; Bohineust, A.; Hivroz, C.; Henry, N. Force Generation upon T Cell Receptor Engagement. *PLoS One* **2011**, *6* (5). <https://doi.org/10.1371/journal.pone.0019680>.
- (47) Liu, B.; Chen, W.; Evavold, B. D.; Zhu, C. Accumulation of Dynamic Catch Bonds between TCR and Agonist Peptide-MHC Triggers T Cell Signaling. *Cell* **2014**, *157* (2), 357–368. <https://doi.org/10.1016/j.cell.2014.02.053>.
- (48) Chesla, S. E.; Selvaraj, P.; Zhu, C. *Measuring Two-Dimensional Receptor-Ligand Binding Kinetics by Micropipette*; 1998.
- (49) Huang, J.; Chen, J.; Chesla, S. E.; Yago, T.; Mehta, P.; McEver, R. P.; Zhu, C.; Long, M. Quantifying the Effects of Molecular Orientation and Length on Two-Dimensional Receptor-Ligand Binding Kinetics\*. *Journal of Biological Chemistry* **2004**, *279* (43), 44915–44923. <https://doi.org/https://doi.org/10.1074/jbc.M407039200>.
- (50) Chen, W.; Evans, E. A.; McEver, R. P.; Zhu, C. Monitoring Receptor-Ligand Interactions between Surfaces by Thermal Fluctuations. *Biophys J* **2008**, *94* (2), 694–701. <https://doi.org/https://doi.org/10.1529/biophysj.107.117895>.
- (51) Wu, L.; Xiao, B.; Jia, X.; Zhang, Y.; Lü, S.; Chen, J.; Long, M. Impact of Carrier Stiffness and Microtopology on Two-Dimensional Kinetics of P-Selectin and P-Selectin Glycoprotein Ligand-1 (PSGL-1) Interactions\*. *Journal of Biological Chemistry* **2007**, *282* (13), 9846–9854. <https://doi.org/https://doi.org/10.1074/jbc.M609219200>.
- (52) Waugh, R. E.; Lomakina, E. B. Active Site Formation, Not Bond Kinetics, Limits Adhesion Rate between Human Neutrophils and Immobilized Vascular Cell Adhesion Molecule 1. *Biophys J* **2009**, *96* (1), 268–275. <https://doi.org/https://doi.org/10.1016/j.bpj.2008.09.009>.
- (53) Zhang, F.; Marcus, W. D.; Goyal, N. H.; Selvaraj, P.; Springer, T. A.; Zhu, C. Two-Dimensional Kinetics Regulation of  $\text{AL}\beta 2$ -ICAM-1 Interaction by Conformational Changes of the AL-Inserted Domain\*. *Journal of Biological Chemistry* **2005**, *280* (51), 42207–42218. <https://doi.org/https://doi.org/10.1074/jbc.M510407200>.
- (54) Lomakina, E. B.; Waugh, R. E. Adhesion Between Human Neutrophils and Immobilized Endothelial Ligand Vascular Cell Adhesion Molecule 1: Divalent Ion Effects. *Biophys J* **2009**, *96* (1), 276–284. <https://doi.org/https://doi.org/10.1016/j.bpj.2008.10.001>.

- (55) Wasserman, H. A.; Beal, C. D.; Zhang, Y.; Jiang, N.; Zhu, C.; Evavold, B. D. MHC Variant Peptide-Mediated Anergy of Encephalitogenic T Cells Requires SHP-11. *The Journal of Immunology* **2008**, *181* (10), 6843–6849. <https://doi.org/10.4049/jimmunol.181.10.6843>.
- (56) Jiang, N.; Huang, J.; Edwards, L. J.; Liu, B.; Zhang, Y.; Beal, C. D.; Evavold, B. D.; Zhu, C. Two-Stage Cooperative T Cell Receptor–Peptide Major Histocompatibility Complex–CD8 Trimolecular Interactions Amplify Antigen Discrimination. *Immunity* **2011**, *34* (1), 13–23. <https://doi.org/https://doi.org/10.1016/j.immuni.2010.12.017>.
- (57) Sabatino Jr., J. J.; Huang, J.; Zhu, C.; Evavold, B. D. High Prevalence of Low Affinity Peptide–MHC II Tetramer–Negative Effectors during Polyclonal CD4+ T Cell Responses. *Journal of Experimental Medicine* **2011**, *208* (1), 81–90. <https://doi.org/10.1084/jem.20101574>.
- (58) Huang, J.; Edwards, L. J.; Evavold, B. D.; Zhu, C. Kinetics of MHC–CD8 Interaction at the T Cell Membrane1. *The Journal of Immunology* **2007**, *179* (11), 7653–7662. <https://doi.org/10.4049/jimmunol.179.11.7653>.
- (59) Chesla, S. E.; Li, P.; Nagarajan, S.; Selvaraj, P.; Zhu, C. The Membrane Anchor Influences Ligand Binding Two-Dimensional Kinetic Rates and Three-Dimensional Affinity of FcγRIII (CD16)\*. *Journal of Biological Chemistry* **2000**, *275* (14), 10235–10246. <https://doi.org/https://doi.org/10.1074/jbc.275.14.10235>.
- (60) Williams, T. E.; Nagarajan, S.; Selvaraj, P.; Zhu, C. Concurrent and Independent Binding of Fcγ Receptors IIa and IIIb to Surface-Bound IgG. *Biophys J* **2000**, *79* (4), 1867–1875. [https://doi.org/https://doi.org/10.1016/S0006-3495\(00\)76436-8](https://doi.org/https://doi.org/10.1016/S0006-3495(00)76436-8).
- (61) Williams, T. E.; Selvaraj, P.; Zhu, C. Concurrent Binding to Multiple Ligands: Kinetic Rates of CD16b for Membrane-Bound IgG1 and IgG2. *Biophys J* **2000**, *79* (4), 1858–1866. [https://doi.org/https://doi.org/10.1016/S0006-3495\(00\)76435-6](https://doi.org/https://doi.org/10.1016/S0006-3495(00)76435-6).
- (62) Williams, T. E.; Nagarajan, S.; Selvaraj, P.; Zhu, C. Quantifying the Impact of Membrane Microtopology on Effective Two-Dimensional Affinity\*210. *Journal of Biological Chemistry* **2001**, *276* (16), 13283–13288. <https://doi.org/https://doi.org/10.1074/jbc.M010427200>.
- (63) Zarnitsyna, V. I.; Zhu, C. Adhesion Frequency Assay for In Situ Kinetics Analysis of Cross-Junctional Molecular Interactions at the Cell-Cell Interface. *JoVE* **2011**, No. 57, e3519. <https://doi.org/doi:10.3791/3519>.
- (64) Rudolph, M. G.; Wilson, I. A. The Specificity of TCR/PMHC Interaction. *Curr Opin Immunol* **2002**, *14* (1), 52–65. [https://doi.org/https://doi.org/10.1016/S0952-7915\(01\)00298-9](https://doi.org/https://doi.org/10.1016/S0952-7915(01)00298-9).
- (65) Chen, Y.; Liu, B.; Ju, L.; Hong, J.; Ji, Q.; Chen, W.; Zhu, C. Fluorescence Biomembrane Force Probe: Concurrent Quantitation of Receptor–Ligand Kinetics and Binding-Induced Intracellular Signaling on a Single Cell. *Journal of Visualized Experiments* **2015**, *2015* (102), 1–13. <https://doi.org/10.3791/52975>.
- (66) Simon, S. I.; Nyunt, T.; Florine-Casteel, K.; Ritchie, K.; Ting-Beall, H. P.; Evans, E.; Needham, D. Dynamics of Neutrophil Membrane Compliance and Microstructure Probed with a Micropipet-Based Piconewton Force Transducer. *Ann Biomed Eng* **2007**, *35* (4), 595–604. <https://doi.org/10.1007/s10439-007-9260-7>.
- (67) Chen, W.; Zarnitsyna, V. I.; Sarangapani, K. K.; Huang, J.; Zhu, C. Measuring Receptor–Ligand Binding Kinetics on Cell Surfaces: From Adhesion Frequency to Thermal Fluctuation Methods. *Cell Mol Bioeng* **2008**, *1* (4), 276. <https://doi.org/10.1007/s12195-008-0024-8>.
- (68) Shen, B.; Zhao, X.; O’Brien, K. A.; Stojanovic-Terpo, A.; Delaney, M. K.; Kim, K.; Cho, J.; Lam, S. C.-T.; Du, X. A Directional Switch of Integrin Signalling and a New Anti-Thrombotic Strategy. *Nature* **2013**, *503* (7474), 131–135. <https://doi.org/10.1038/nature12613>.
- (69) Yago, T.; Lou, J.; Wu, T.; Yang, J.; Miner, J. J.; Coburn, L.; López, J. A.; Cruz, M. A.; Dong, J.-F.; McIntire, L. v.; McEver, R. P.; Zhu, C. Platelet Glycoprotein Iba Forms Catch Bonds with

- Human WT VWF but Not with Type 2B von Willebrand Disease VWF. *J Clin Invest* **2008**, *118* (9), 3195–3207. <https://doi.org/10.1172/JCI35754>.
- (70) Ruggeri, Z. M. Platelets in Atherothrombosis. *Nat Med* **2002**, *8* (11), 1227–1234. <https://doi.org/10.1038/nm1102-1227>.
- (71) Evans, E.; Leung, A.; Heinrich, V.; Zhu, C. Mechanical Switching and Coupling between Two Dissociation Pathways in a P-Selectin Adhesion Bond. *Proceedings of the National Academy of Sciences* **2004**, *101* (31), 11281–11286. <https://doi.org/10.1073/pnas.0401870101>.
- (72) Chen, W.; Lou, J.; Zhu, C. Forcing Switch from Short- to Intermediate- and Long-Lived States of the AA Domain Generates LFA-1/ICAM-1 Catch Bonds. *Journal of Biological Chemistry* **2010**, *285* (46), 35967–35978. <https://doi.org/10.1074/jbc.M110.155770>.
- (73) Chen, W.; Lou, J.; Evans, E. A.; Zhu, C. Observing Force-Regulated Conformational Changes and Ligand Dissociation from a Single Integrin on Cells. *Journal of Cell Biology* **2012**, *199* (3), 497–512. <https://doi.org/10.1083/jcb.201201091>.
- (74) Wu, P.; Zhang, T.; Liu, B.; Fei, P.; Cui, L.; Qin, R.; Zhu, H.; Yao, D.; Martinez, R. J.; Hu, W.; An, C.; Zhang, Y.; Liu, J.; Shi, J.; Fan, J.; Yin, W.; Sun, J.; Zhou, C.; Zeng, X.; Xu, C.; Wang, J.; Evavold, B. D.; Zhu, C.; Chen, W.; Lou, J. Mechano-Regulation of Peptide-MHC Class I Conformations Determines TCR Antigen Recognition. *Mol Cell* **2019**, *73* (5), 1015–1027.e7. <https://doi.org/https://doi.org/10.1016/j.molcel.2018.12.018>.
- (75) Zhu, C.; Jiang, N.; Huang, J.; Zarnitsyna, V. I.; Evavold, B. D. Insights from in Situ Analysis of TCR–PMHC Recognition: Response of an Interaction Network. *Immunol Rev* **2013**, *251* (1), 49–64. <https://doi.org/https://doi.org/10.1111/imr.12016>.
- (76) Heinrich, V.; Leung, A.; Evans, E. Nano- to Microscale Dynamics of p-Selectin Detachment from Leukocyte Interfaces. II. Tether Flow Terminated by p-Selectin Dissociation from PSGL-1. *Biophys J* **2005**, *88* (3), 2299–2308. <https://doi.org/10.1529/biophysj.104.051706>.
- (77) Pang, A.; Cui, Y.; Chen, Y.; Cheng, N.; Delaney, M. K.; Gu, M.; Stojanovic-Terpo, A.; Zhu, C.; Du, X. Shear-Induced Integrin Signaling in Platelet Phosphatidylserine Exposure, Microvesicle Release, and Coagulation. *Blood* **2018**, *132* (5), 533–543. <https://doi.org/10.1182/blood-2017-05-785253>.
- (78) Mazzucato, M.; Pradella, P.; Cozzi, M. R.; de Marco, L.; Ruggeri, Z. M. Sequential Cytoplasmic Calcium Signals in a 2-Stage Platelet Activation Process Induced by the Glycoprotein Iba $\alpha$  Mechanoreceptor. *Blood* **2002**, *100* (8), 2793–2800. <https://doi.org/10.1182/blood-2002-02-0514>.
- (79) Nesbitt, W. S.; Kulkarni, S.; Giuliano, S.; Goncalves, I.; Dopheide, S. M.; Yap, C. L.; Harper, I. S.; Salem, H. H.; Jackson, S. P. Distinct Glycoprotein Ib/V/IX and Integrin AIIb $\beta$ 3-Dependent Calcium Signals Cooperatively Regulate Platelet Adhesion under Flow. *Journal of Biological Chemistry* **2002**, *277* (4), 2965–2972. <https://doi.org/10.1074/jbc.M110070200>.
- (80) Ju, L.; McFadyen, J. D.; Al-Daher, S.; Alwis, I.; Chen, Y.; Tønnesen, L. L.; Maiocchi, S.; Coulter, B.; Calkin, A. C.; Felner, E. I.; Cohen, N.; Yuan, Y.; Schoenwaelder, S. M.; Cooper, M. E.; Zhu, C.; Jackson, S. P. Compression Force Sensing Regulates Integrin AIIb $\beta$ 3 Adhesive Function on Diabetic Platelets. *Nat Commun* **2018**, *9* (1). <https://doi.org/10.1038/s41467-018-03430-6>.
- (81) Zhou, F.; Zhang, F.; Zarnitsyna, V. I.; Doudy, L.; Yuan, Z.; Li, K.; McEver, R. P.; Lu, H.; Zhu, C. The Kinetics of E-Selectin- And P-Selectin-Induced Intermediate Activation of Integrin AII $\beta$ 2 on Neutrophils. *J Cell Sci* **2021**, *134* (18). <https://doi.org/10.1242/jcs.258046>.
- (82) Sibener, L. v.; Fernandes, R. A.; Kolawole, E. M.; Carbone, C. B.; Liu, F.; McAfee, D.; Birnbaum, M. E.; Yang, X.; Su, L. F.; Yu, W.; Dong, S.; Gee, M. H.; Jude, K. M.; Davis, M. M.; Groves, J. T.; Goddard, W. A.; Heath, J. R.; Evavold, B. D.; Vale, R. D.; Garcia, K. C. Isolation of

- a Structural Mechanism for Uncoupling T Cell Receptor Signaling from Peptide-MHC Binding. *Cell* **2018**, *174* (3), 672-687.e27. <https://doi.org/10.1016/j.cell.2018.06.017>.
- (83) Qin, R.; An, C.; Chen, W. Physical-Chemical Regulation of Membrane Receptors Dynamics in Viral Invasion and Immune Defense. *J Mol Biol* **2023**, *435* (1), 167800. <https://doi.org/https://doi.org/10.1016/j.jmb.2022.167800>.
- (84) Chakraborty, A. K.; Weiss, A. Insights into the Initiation of TCR Signaling. *Nat Immunol* **2014**, *15* (9), 798–807. <https://doi.org/10.1038/ni.2940>.
- (85) Chen, Y.; Lee, H.; Tong, H.; Schwartz, M.; Zhu, C. Force Regulated Conformational Change of Integrin AV $\beta$ 3. *Matrix Biology* **2017**, *60–61*, 70–85. <https://doi.org/10.1016/j.matbio.2016.07.002>.
- (86) Sawicka, A.; Babataheri, A.; Dogniaux, S.; Barakat, A. I.; Gonzalez-Rodriguez, D.; Hivroz, C.; Husson, J. Micropipette Force Probe to Quantify Single-Cell Force Generation: Application to T-Cell Activation. *Mol Biol Cell* **2017**, *28* (23), 3229–3239. <https://doi.org/10.1091/mbc.E17-06-0385>.
- (87) Zhu, C.; Chen, W.; Lou, J.; Rittase, W.; Li, K. Mechanosensing through Immunoreceptors. *Nat Immunol* **2019**, *20* (10), 1269–1278. <https://doi.org/10.1038/s41590-019-0491-1>.
- (88) Simon, S. I.; Nyunt, T.; Florine-Casteel, K.; Ritchie, K.; Ting-Beall, H. P.; Evans, E.; Needham, D. Dynamics of Neutrophil Membrane Compliance and Microstructure Probed with a Micropipet-Based Piconewton Force Transducer. *Ann Biomed Eng* **2007**, *35* (4), 595–604. <https://doi.org/10.1007/s10439-007-9260-7>.
- (89) Zhu, C.; Bao, G.; Wang, N. Cell Mechanics Mechanical Response Cell Adhesion and Molecular Deformation. *Annu Rev Biomed Eng* **2000**, *2* (1), 189–226.
- (90) Taubenberger, A. v.; Hutmacher, D. W.; Muller, D. J. Single-Cell Force Spectroscopy, an Emerging Tool to Quantify Cell Adhesion to Biomaterials. *Tissue Eng Part B Rev* **2014**, *20* (1), 40–55. <https://doi.org/10.1089/ten.teb.2013.0125>.
- (91) Chen, Y.; Ju, L.; Rushdi, M.; Ge, C.; Zhu, C. Receptor-Mediated Cell Mechanosensing. *Mol Biol Cell* **2017**, *28* (23), 3134–3155. <https://doi.org/10.1091/mbc.E17-04-0228>.
- (92) Kim, J.; Shin, J. H. Stable, Free-Space Optical Trapping and Manipulation of Sub-Micron Particles in an Integrated Microfluidic Chip. *Sci Rep* **2016**, *6* (1), 33842. <https://doi.org/10.1038/srep33842>.
- (93) MacDonald, M. P.; Spalding, G. C.; Dholakia, K. Microfluidic Sorting in an Optical Lattice. *Nature* **2003**, *426* (6965), 421–424. <https://doi.org/10.1038/nature02144>.
- (94) Xu, Z.; Song, W.; Crozier, K. B. Optical Trapping of Nanoparticles Using All-Silicon Nanoantennas. *ACS Photonics* **2018**, *5* (12), 4993–5001. <https://doi.org/10.1021/acsp Photonics.8b01250>.
- (95) Chen, Z.; Lu, J.; Zhang, C.; Hsia, I.; Yu, X.; Marecki, L.; Marecki, E.; Asmani, M.; Jain, S.; Neelamegham, S.; Zhao, R. Microclot Array Elastometry for Integrated Measurement of Thrombus Formation and Clot Biomechanics under Fluid Shear. *Nat Commun* **2019**, *10* (1), 2051. <https://doi.org/10.1038/s41467-019-10067-6>.
- (96) Myrand-Lapierre, M. E.; Deng, X.; Ang, R. R.; Matthews, K.; Santoso, A. T.; Ma, H. Multiplexed Fluidic Plunger Mechanism for the Measurement of Red Blood Cell Deformability. *Lab Chip* **2015**, *15* (1), 159–167. <https://doi.org/10.1039/c4lc01100g>.
- (97) Mak, M.; Erickson, D. A Serial Micropipette Microfluidic Device with Applications to Cancer Cell Repeated Deformation Studies. *Integrative Biology* **2013**, *5* (11), 1374–1384. <https://doi.org/10.1039/c3ib40128f>.

- (98) Sgouralis, I.; Whitmore, M.; Lapidus, L.; Comstock, M. J.; Pressé, S. Single Molecule Force Spectroscopy at High Data Acquisition: A Bayesian Nonparametric Analysis. *J Chem Phys* **2018**, *148* (12), 123320. <https://doi.org/10.1063/1.5008842>.
- (99) Hines, W. C.; Yaswen, P.; Bissell, M. J. Modelling Breast Cancer Requires Identification and Correction of a Critical Cell Lineage-Dependent Transduction Bias. *Nat Commun* **2015**, *6* (1), 6927. <https://doi.org/10.1038/ncomms7927>.
- (100) Lee, S.; Kwon, O.; Jeon, M.; Song, J.; Shin, S.; Kim, H.; Jo, M.; Rim, T.; Doh, J.; Kim, S.; Son, J.; Kim, Y.; Kim, C. Super-Resolution Visible Photoactivated Atomic Force Microscopy. *Light Sci Appl* **2017**, *6* (11), e17080–e17080. <https://doi.org/10.1038/lsa.2017.80>.
- (101) Šmít, D.; Fouquet, C.; Doulazmi, M.; Pincet, F.; Trembleau, A.; Zapotocky, M. BFPTool: A Software Tool for Analysis of Biomembrane Force Probe Experiments. *BMC Biophys* **2017**, *10* (1). <https://doi.org/10.1186/s13628-016-0033-2>.
- (102) Pincet, F.; Husson, J. The Solution to the Streptavidin-Biotin Paradox: The Influence of History on the Strength of Single Molecular Bonds. *Biophys J* **2005**, *89* (6), 4374–4381. <https://doi.org/10.1529/biophysj.105.067769>.

## Tables

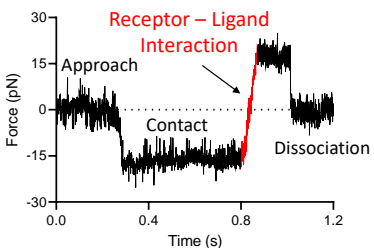
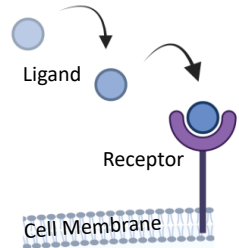
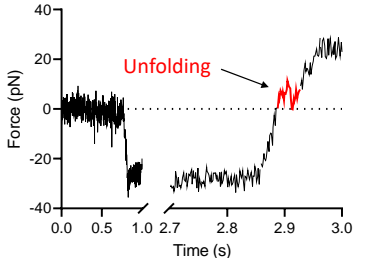
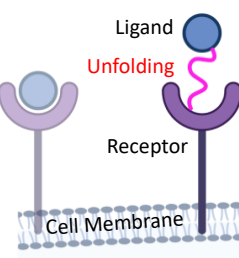
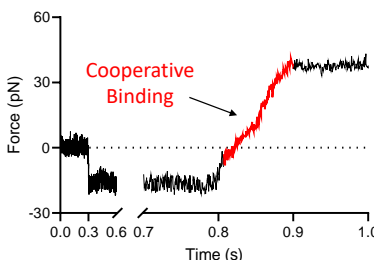
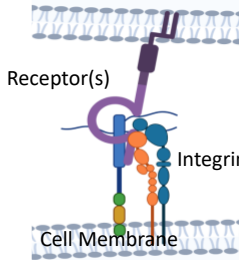
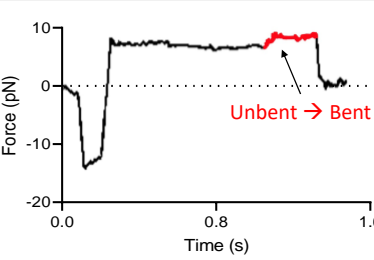
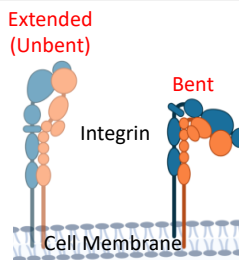
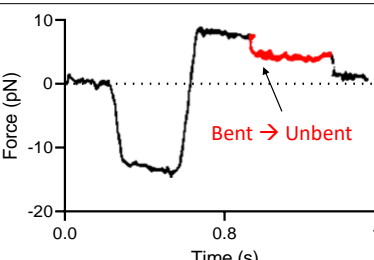
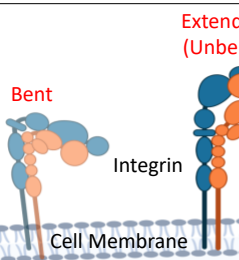
**Table 1. Key mechanical variables of BFP dynamic force spectroscopies.** A range of parameters can be customized during BFP experiments. The columns show parameters, definitions of parameters, force vs time curve representation, and schematic representation of key variables. Row 1 presents the contact time ( $t_c$ ) of 0.1s (*magenta*) and 0.2s (*green*). Row 2 presents the impingement force ( $f_c$ ) of 20 pN (*magenta*) and 50 pN (*green*) and Row 3 presents the ramping rate ( $r_f$ ) of  $10^2$  pN/s (*grey*),  $10^3$  pN/s (*magenta*), and  $10^4$  pN/s (*green*).

Parameter	Definition	Force vs. time curve representation	Schematic representation
Contact time $t_c$ (s)	The duration for the target bead/cell to stay in contact with the probe bead.		
Impingement force $f_c$ (pN)	The magnitude of force that the target bead/cell impinges the probe bead at.		
Ramping rate $r_f$ (pN/s)	How fast the target bead/cell retracts after impingement.		

**Table 2. Key measurements obtained through BFP.** The columns show the measurement, the representation of force vs. time curves, the schematic representation, and the data analysis details. In a touch cycle, the target cell/bead impinges the probe bead on the RBC. This impingement causes the RBC to deflect in the x-plane, which is represented by the force vs. time curve during a BFP experiment (Column 2). The impingement is represented by a negative force (*magenta*). When the target cell/bead is retracted, the RBC is pulled if a bond has formed between the receptor-ligand pair. This manifests as a positive deflection in the x-plane and is represented by a position force (*green*). In an adhesion event, the bond between the receptor-ligand pair quickly dissociates, and the force returns to its starting position ( $x = 0$ ) and returns to baseline ( $F = 0$  pN) quickly (Row 1). If a tether forms, the cell membrane is separated from the cytoskeleton as the crossover force  $f_{\otimes}$  is reached (Row 2). The time duration in which the tether is maintained is the bond lifetime (Row 3).

Measurement	Force vs. time curve representation	Schematic representation	Data analysis
Adhesion Frequency ( $P_a$ ) $P_a = \frac{\text{Number of adhesion event}}{\text{Total event}}$			Sequentially inspect each cycle's force vs. time signal and record cycles that contain an adhesion event. Calculate the average adhesion frequency from all repeats.
Tether Frequency ( $P_{\text{tether}}$ ) $P_{\text{tether}} = \frac{\text{Number of tether event}}{\text{Total event}}$ Crossover force ( $f_{\otimes}$ )			Sequentially inspect each cycle's force vs. time signal and record cycles that contain a tether event. Calculate the average tether frequency from all repeats.
Bond Lifetime = $t_d - t_a$			Record the duration of the bond from its association to dissociation as bond lifetime.

**Table 3. Receptor-ligand binding events and illustrative BFP force vs time curves.** The table shows different types of receptor-ligand interactions that can be characterized using BFP, along with schematic representations and illustrative force vs. time curves. Column 1 lists the type of interaction, while column 2 shows the force vs. time curves, and column 3 provides the corresponding schematic. The interactions include receptor-ligand binding, receptor unfolding, receptor cooperative binding, receptor bending, and receptor unbending.

Bond behaviors	Representative DFS signatures	Schematics
(1) Receptor-Ligand Interaction		
(2) Receptor Unfolding		
(3) Receptor Cooperative Binding		
(4) Receptor Bending		
(5) Receptor Unbending		

**Table 4. Conventional BFP configurations and applications.** Column 1 lists the application, while column 2 provides the corresponding schematic, and column 3 lists the key findings of the application. Some of the applications include the characterization of von-Willebrand factor (VWF) and platelet receptor glycoprotein Ib (GPIb)<sup>17,26,29,30</sup> in thrombosis, T-cell receptor (TCR) and peptide-major histocompatibility complex (pMHC)<sup>19,33,74,75</sup> interaction in immunology, and neutrophil receptor interactions in inflammation<sup>15,16,21,37,76</sup>.

Application	Thrombosis	Immunology	Inflammation
Cell Type	Platelet	T cell	Neutrophil
Receptor—Ligand axes	VWF—GPIb $\alpha$	pMHC—TCR	P-selectin—PSGL-1, ICAM-1—LFA-1
BFP Configurations			
Significance	<ul style="list-style-type: none"> <li>Characterized the force induced conformational changes in VWF-A1—GPIb<math>\alpha</math> complexes.</li> <li>Confirmed the existence of juxtamembrane mechanosensitive domain (MSD).</li> <li>Observed the unfolding of the LRRD and MSD of GPIb<math>\alpha</math></li> <li>Discovered that VWF activation can be induced via hemodynamic force</li> </ul>	<ul style="list-style-type: none"> <li>Magnitude and duration of force are important to prolong pMHC-TCR bond lifetime and lead to conformational change</li> <li>Revealed the dynamic mechano-chemical coupling mechanism of pMHC-TCR catch bond.</li> <li>Shed light on T cell selection in adaptive immunity mechano-regulation</li> </ul>	<ul style="list-style-type: none"> <li>Observed a three-step of P-selectin-PSGL-1 bond dissociation</li> <li>Observed real-time reversible conformational switch of LFA-1 between bent and extended. LFA-1 conformation and force regulate the ICAM-1-LFA-1 kinetics.</li> <li>Discovered enhanced LFA-1-ICAM-1 catch bond behavior at 10 pN</li> </ul>

**Table 5. Dual BFP configurations and applications.** Column 1 lists the application, while column 2 provides the corresponding schematic, and column 3 lists the key findings of the application. Some of the applications include using two probe beads to sequentially engage two ligands on a platelet<sup>27,45,80</sup>, and to study T-cell<sup>81</sup> activation by spatial crosstalk.

Application	Thrombosis	Immunology
Cell Type	Platelet	T Cell
Receptor—Ligand axes	Temporal crosstalk: VWF—GPIb $\alpha$ and Fibronectin— $\alpha_{IIb}\beta_3$	Spatial crosstalk: pMHC—TCR, ICAM-1—LFA-1
BFP Configurations		
Significance	<ul style="list-style-type: none"> <li>The combination of dual BFP and fBFP revealed the role of GPIb<math>\alpha</math> in mechanoreception</li> <li>Discovered the intermediate state of integrin <math>\alpha_{IIb}\beta_3</math> (extended-closed) and the 'outside-in' mechanosignalling pathway.</li> <li>The 'Switch' assay setting was then combined with compression assay to reveal the compression force regulation of on diabetic platelet</li> </ul>	<ul style="list-style-type: none"> <li>Extended previous concept on pMHC-TCR interaction</li> <li>Revealed that the TCR-induced LFA-1 activation is a global process, where pMHC-TCR interaction triggers global and sustained upregulation of LFA-1 binding affinity</li> </ul>

**Table 6. Fluorescence BFP configurations and applications.** Column 1 lists the application, while column 2 provides the corresponding schematic, and column 3 lists the key findings of the application. Some of the applications include using fBFP to observe the intraplatelet  $\text{Ca}^{2+}$  flux during the GPIb unfolding process in thrombosis<sup>26,27</sup>, and to observe intracellular  $\text{Ca}^{2+}$  levels alteration in T-cells during the TCR-pMHC binding process in immunology<sup>82-84</sup>.

Application	Thrombosis	Immununology
Cell Type	Platelet	T Cell
Receptor—Ligand axes	VWF—GPIb	pMHC—TCR
BFP Configurations	<p> <span style="color: red;">●</span> RBC    <span style="color: pink;">●</span> Platelet    <span style="color: blue;">—</span> GPIbα  <span style="color: grey;">●</span> Bead    <span style="color: green;">●</span> VWF-A1         </p>	<p> <span style="color: red;">●</span> RBC    <span style="color: green;">●</span> T Cell    <span style="color: blue;">—</span> TCR  <span style="color: grey;">●</span> Bead    <span style="color: orange;">—</span> pMHC         </p>
Significance	<ul style="list-style-type: none"> <li>Discovered that LRRD unfolding prolongs VWF-A1—GPIbα bond lifetime to facilitate MSD unfolding</li> <li>Revealed the intermediate state of platelet integrin <math>\alpha_{\text{Ib}}\beta_3</math> for the first time</li> <li>Correlated intraplatelet <math>\text{Ca}^{2+}</math> level to the force induced LRRD unfolding, extending the scope of platelet signalling research</li> <li>Achieved single platelet manipulation and in situ VWF-A1—GPIbα binding kinetics characterization</li> </ul>	<ul style="list-style-type: none"> <li>Early and rapid accumulation of pMHC-TCR bond lifetime contribute to T cell signaling triggering.</li> <li>Agonist-specific catch bonds prolonged pMHC-TCR lifetime under optimal force (bond strengthening) and triggered <math>\text{Ca}^{2+}</math>, hence T cell signaling</li> <li>Digitalized and visualized the TCR activation process, which led the membrane receptor mechanosensing and signaling research into a new era</li> </ul>

**Table 7. Modified BFP configurations and applications.** Column 1 lists the application, while column 2 provides the corresponding schematic, and column 3 lists the key findings of the application. Some of the applications include using a modified dual BFP setup to activate platelets with adenosine diphosphate (ADP) before engaging a soluble and an immobilized ligand on the probe<sup>17</sup> and using an ultra-stable BFP to achieve higher accuracy on force determination for bond lifetimes beyond 200s in force clamp assay<sup>41,83</sup>.

Upgrades	Replace Probe with an agonist reservoir	Ultra-stable BFP
Application	Thrombosis	Cancer Biology
Cell Types	Platelet	T cell
Receptor— Ligand axes	P <sub>2</sub> Y receptor, CD62p	PD-1
BFP Configurations		
Significance	<ul style="list-style-type: none"> <li>ADP stimulation of the P<sub>2</sub>Y agonist receptor upregulated the platelet activation marker CD62p and displayed higher binding to the anti-CD62p compared to the pre-stimulated platelets</li> <li>Provided evidence for signaling events can be initiated by soluble agonist binding to a surface receptor, hence upregulating the expression or function of another receptor</li> </ul>	<ul style="list-style-type: none"> <li>Developed and incorporated a smart control feedback system into the force clamp assay to measure bond lifetimes beyond 200s, resolved the probe drifting issue in the conventional setup, leading to more accurate force determination</li> <li>Combined with MD simulation to predict the protein–protein interaction binding site, leading towards the new era of single cell mechanobiology study</li> </ul>